buildings

MDPI

Article

Geospatial Assessment of Solar Energy Potential: Utilizing MATLAB and UAV-Derived Datasets

Nava Sai Divya Ryali [1,*], Nitin Kumar Tripathi [1], Sarawut Ninsawat [1] and Jai Govind Singh [2]

[1] Department of Information and Communication Technologies, School of Engineering and Technology, Asian Institute of Technology, Pathum Thani 12120, Thailand; nitinkt@ait.ac.th (N.K.T.); sarawutn@ait.ac.th (S.N.)
[2] Department of Energy, Environment and Climate Change, School of Environment, Resources and Development, Asian Institute of Technology, Pathum Thani 12120, Thailand; jgsingh@ait.ac.th
* Correspondence: st122378@ait.asia

Abstract: Solar energy is playing a crucial role in easing the burden of environmental protection and depletion of conventional energy resources. The use of solar energy in urban settings is essential to meet the growing energy demand and achieve sustainable development goals. This research assesses the solar potential of buildings considering shading events and analyzes the impact of urban built forms (UBFs) on incoming solar potential. The primary data for constructing a virtual 3D city model are derived from a UAV survey, utilizing drone deployment software for flight planning and image acquisition. Geospatial modelling was conducted using the MATLAB Mapping Toolbox to simulate solar irradiation on all the building envelopes in the study area in Jamshedpur, India. The empirical investigation quantified annual solar potential for more than 30,000 buildings in the region by considering time-varying shadowing events based on the sun's path. The region's annual solar energy of 310.149 TWh/year is estimated. Integrating UAV-derived datasets with MATLAB introduces a cost-effective and accurate approach, offering to develop 3D city models, assess solar potential, and correlate the impact of urban building forms (UBFs) to incoming solar potential.

Keywords: 3D city model; spatial analysis; solar potential; unmanned aerial vehicle; rooftop and facades

Citation: Ryali, N.S.D.; Tripathi, N.K.; Ninsawat, S.; Singh, J.G. Geospatial Assessment of Solar Energy Potential: Utilizing MATLAB and UAV-Derived Datasets. *Buildings* **2024**, *14*, 1781. https://doi.org/10.3390/buildings14061781

Academic Editor: Xingxing Zhang

Received: 21 April 2024
Revised: 6 June 2024
Accepted: 10 June 2024
Published: 13 June 2024

1. Introduction

India has recently outperformed most economies globally, and it is imperative to ensure sustainable growth. The drive to grow the economy comes with a massive demand for energy and resources, pending environmental stress from waste production and resource extraction [1]. The most important economic growth, human prosperity, and development goals are energy access and transition to sustainable energy [2]. An unbroken supply of clean, renewable energy is essential to counteract climate change and environmental deterioration to promote social progress and economic prosperity [3].

One of the country's ambitious goals is to achieve 500 GW of non-fossil fuel energy capacity by 2030, where 280 GW must be from solar energy. Furthermore, India desires to reduce the economy's carbon intensity by 45% and carbon emissions by one billion tons by 2030. Notably, India's top priority is to attain net-zero emissions by 2070 [4]. According to MNRE-GEF-UNIDO, India has achieved remarkable progress in renewable energy deployment, increasing installed capacity from 3.5 GW in 2002 to around 80.4 GW (excluding big hydro) in June 2019 [3]. As of 31 December 2022, 167.75 GW of renewable energy capacity was installed in the nation. Regarding the installed capacity of solar PV systems, the REN21 Renewables 2022 Global Status Report has indicated India as the fourth place globally [5].

Additionally, India is witnessing a sharp increment in urbanization. The percentage of people living in cities was 28% in 2001, 31% in 2011, and 34% in 2019. According to UN estimates, it will reach 41% in 2030 and almost 50% by 2050. Rapid urbanization has led to unplanned, densely inhabited cities that have significantly altered the urban environment

and have exponentially increased energy consumption [6]. To achieve sustainable development goals, it is imperative to increase the capacity of solar energy utilization in urban settings. Buildings are typically the main structural components of cities and are in energy demand; the practical usage of building surfaces can produce sustainable solar energy [7]. The configuration of settlements and physical characteristics like size, shape, and density are urban built form (UBF) elements [8]. It is critical to assess the practical solar potential and provide optimal placement and sizing of PV systems before deployment, as the Indian cities are unplanned, complex, and have dense concentrations [9].

The newest development in remote sensing for applications like energy mapping, utility mapping, and sustainable urban planning is the 3D modelling of structures. A 3D model's ability to capture the distinctive details of a city can assist people in comprehending both the city's overall layout and visualizing how elements interact [10].

The quality and reliability of the primary data are essential to obtain accurate geometry data and distinctive features of building structures [11]. Low-range remote sensing technology is highly efficient in generating surface models. The 3D city models of the real world are often generated based on survey methods like total station, Global Navigation Satellite System (GNSS), unmanned aerial vehicles (UAVs), Light Detection and Ranging (LIDAR), and other integrated technologies [12]. LiDAR can produce high-resolution point cloud data but is the most expensive for topographic surveys [13]. On the other hand, unmanned aerial vehicles (UAVs) provide accurate and comprehensive elevation data, which can be used to classify land cover and land use precisely when compared with conventional satellite images [14]. UAVs can accomplish significant tasks quickly, accurately, and with higher resolution by generating millions of precise 3D points [15], more than any other satellite data source; the tasks include cadastral surveying, earth engineering, hazard monitoring, automated mapping, corridor surveying, utility mapping, urban mapping, energy mapping, and terrain mapping [16]. UAVs have immense potential for topographical mapping with real-time elevation data [17]. UAVs are used for urban applications and building footprint extractions, allowing the generation of accurate 3D city models and analysis of building structures [18].

Building Energy Modelling is the latest trend in research to assess energy demand and sustainable energy production to estimate potential economic gains of communities [19]. Renewable energy production can be significant in urban areas if buildings are designed, constructed, and operated to maximize energy performance and reduce carbon emissions [20]. Previously, multiple-scale solar energy potential assessments were conducted using various tools and methods, to estimate the two-dimensional solar potential for installing rooftop PV systems [21]. The effective use of PV systems could be achieved by conducting three-dimensional analysis and quantitative mapping of the solar potential of urban surfaces involving building facades/walls along with the rooftops. Photovoltaic generating components can be deployed on building walls/facades and rooftop PV installations if building facades are efficiently used, as building heights in urban areas continue to increase rapidly.

In this study, geospatial modelling and analysis were conducted to compute the solar potential of urban buildings involving walls along with rooftops. The developed model is a comprehensive tool that considers physical, geographical, and technical parameters [22] [23] for assessing solar potential. By considering these factors, the model provides a detailed and accurate analysis of the solar energy potential in the urban context. One crucial aspect considered is the shading patterns caused by surrounding buildings. Shadowing events in urban areas significantly correlate with the solar potential [24] due to the heterogeneous nature of urban built forms and their impact on solar potential [25]. Considering these parameters, the model can provide insights into the optimal placement of PV systems as the analysis provides a statistical correlation between physical parameters and solar potential. Considering these factors, intricate urban details, and interactions, the model offers valuable insights for decision-making processes related to solar energy planning, infrastructure development, and renewable energy integration.

2. Methods and Study Area

A case study is presented in this paper to estimate the solar potential of buildings in Jamshedpur, India. Primary data were taken from the UAV survey to develop a simplified 3D city model. Spatial modelling was carried out using MATLAB 2021b, which was extensively used as a high-performance computational tool to model and solve complex equations of energy systems [26]. Various physical parameters are considered to estimate the incoming solar irradiation. Geographical aspects are evaluated to determine the suitability of the region.

Additionally, technical calculations are performed to calculate the power generation in the study area [27], for example, the duration of sunshine, changes in the sun's path, slope, aspect, site latitude, longitude, and elevation, as well as time-varying shadowing events and climatic conditions. The developed framework to achieve the research objectives is presented in Table 1.

Table 1. Framework of the research objectives.

Objective	Required Data	Tools/Methods
To generate a simplified 3D City Model from the developed surface model using collected high resolution images from UAV	Primary field survey to extract high resolution imagery data latitude and longitude, Dense Point cloud data and Ortho Mosaic	Drone Deploy for mission planning, AGI Soft Metashape for Image stitching and point cloud generation. UAV data Processing. QGIS for feature editing to generate building footprints. Global Mapper for Point cloud data processing for extracting building heights
To carry out spatial modelling using MATLAB to estimate the solar potential for dynamic solar illumination on a simplified 3D City Model	3D City Model with discrete level of detail LoD-1.1	MATLAB Mapping Toolbox
Assessment of the Model with comparison to the experimental results for model Validation	Theoretical Value of Solar Radiation and Real-Time Solar Radiation	Experimental Setup and MATLAB

2.1. Study Area

Jamshedpur is one of India's most populated and well-planned industrial cities. Jamshedpur is in Jharkhand State's southern region at 22°48′ N longitude and 86°12′ E latitude, as shown in Figure 1. This study area is representative of the rapidly urbanizing areas with a considerable population and a high energy demand. Jamshedpur is the center for commercial and industrial activities; one of the largest industries, Tata Iron and Steel Company (TISCO), is in the city.

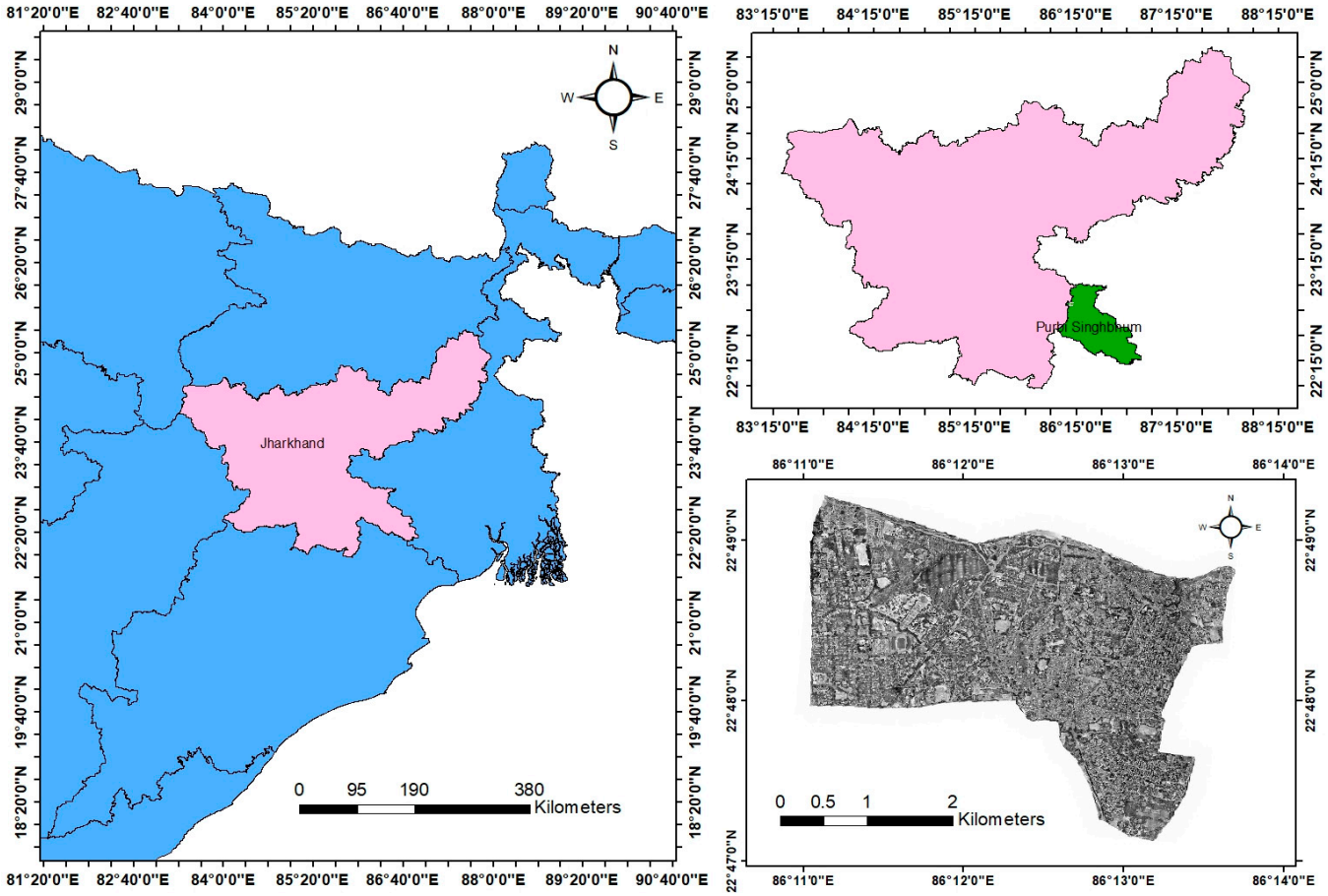

Figure 1. Study area.

2.2. Data Acquisition to Develop 3D City Model

UAVs that serve as terrestrial devices are emerging as data of higher spatial and temporal resolution can be acquired [28]. Additional advantages include minimizing data collection delays, movement flexibility, reduced cost, and effective delivery [29]. UAV image acquisition is used to develop the Digital Surface Model (DSM). A primary field visit has been made to understand the basic scenario of the study area (such as the presence of water, building structures, and vegetation heights). The field visit assisted in detecting static safe landing zones by involving factors like obstacle height and distance. Drone Deploy software was used for mission planning and image acquisition [30]. The flight campaign was carried out at an average flying height of 95 m by a rotorcraft (RPAS) at 10 m/s flight speed and images were captured with a Sony of 1/2.3′CMOS sensor with an effective pixel of 8.29 M and field of view (FOV) of 81.4°. The flight trajectory with a flight direction of 165° is shown in Figure 2a. The flight line is planned with an optimum value for side and frontal overlap of 70 % [31] to avoid data gaps in steep terrains and to maintain image accuracy [32], as illustrated in Figure 2b. Frontal and side overlap should be increased to enhance the mosaic stitching process if the terrain is complex. However, increased overlap may increase the image count, battery consumption, and duration; stitching problems will elevate as more movements will be caught because of moving entities in the capturing area [33]. Therefore, additional post-processing adjustments are required to accommodate large datasets and to enhance the accuracy of the 3D elevation model [34].

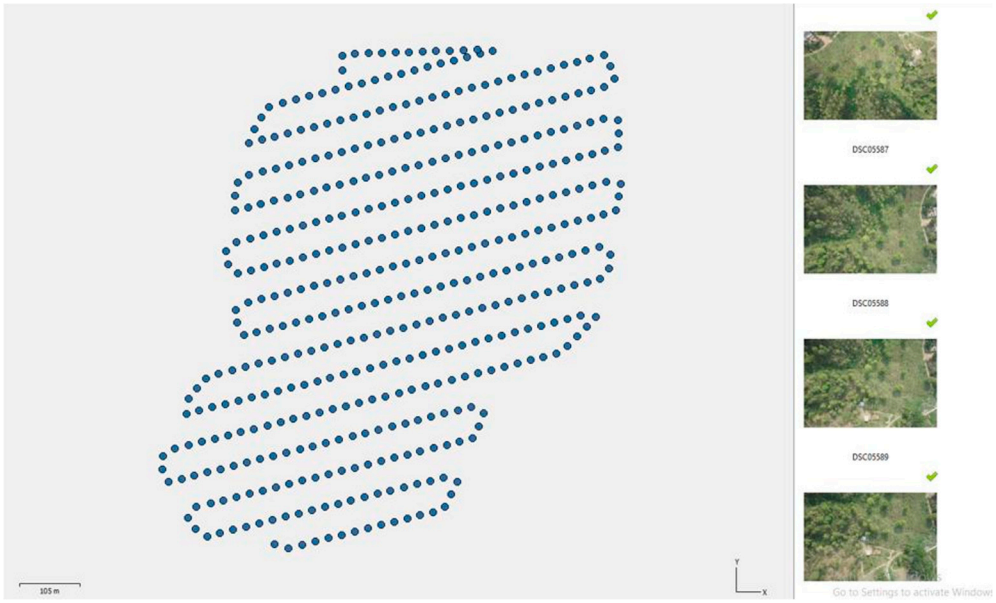

(**a**)

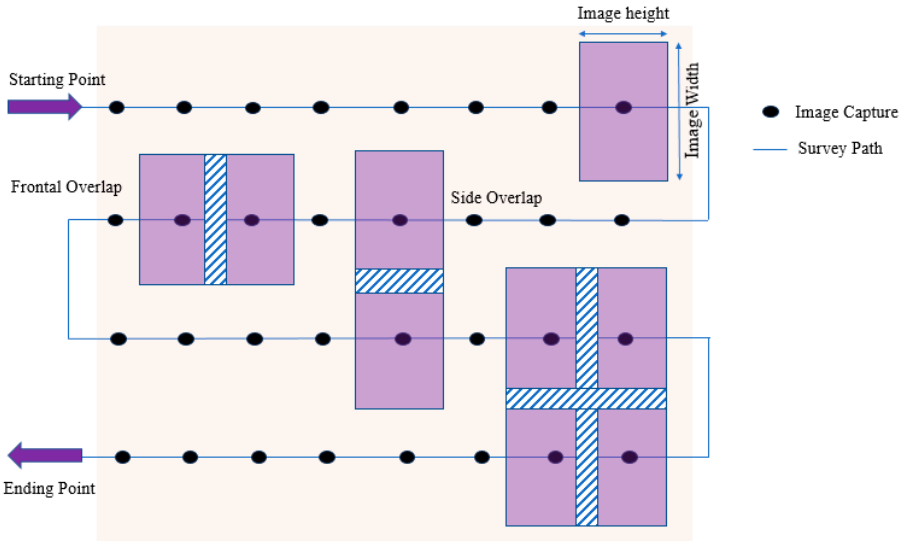

(**b**)

Figure 2. Image accruing system to maintain overlap using UAVs. (**a**) UAV scan path (blue dots) of each image acquired/captured. (**b**) Illustration of overlap in image accruing system.

The UAV survey was conducted over 1 week and has captured 5856 images. The resulting images were processed using AGIsoft Metashape Professional software [35,36] for geo-referencing, geo-correction, building a dense point cloud, and ortho stitching/mosaic operations [37]. The processing time for image stitching and point cloud generation was approx. 24 h. The primary datasets generated from the UAV survey are Ortho Mosaic, which has a 5cm resolution (TIFF file format of size 15.8 GB), and dense point cloud, which has a density of 18 points/m^2 (LAZ file format of size 38.8 GB), and the developed methodology is shown in Figure 3.

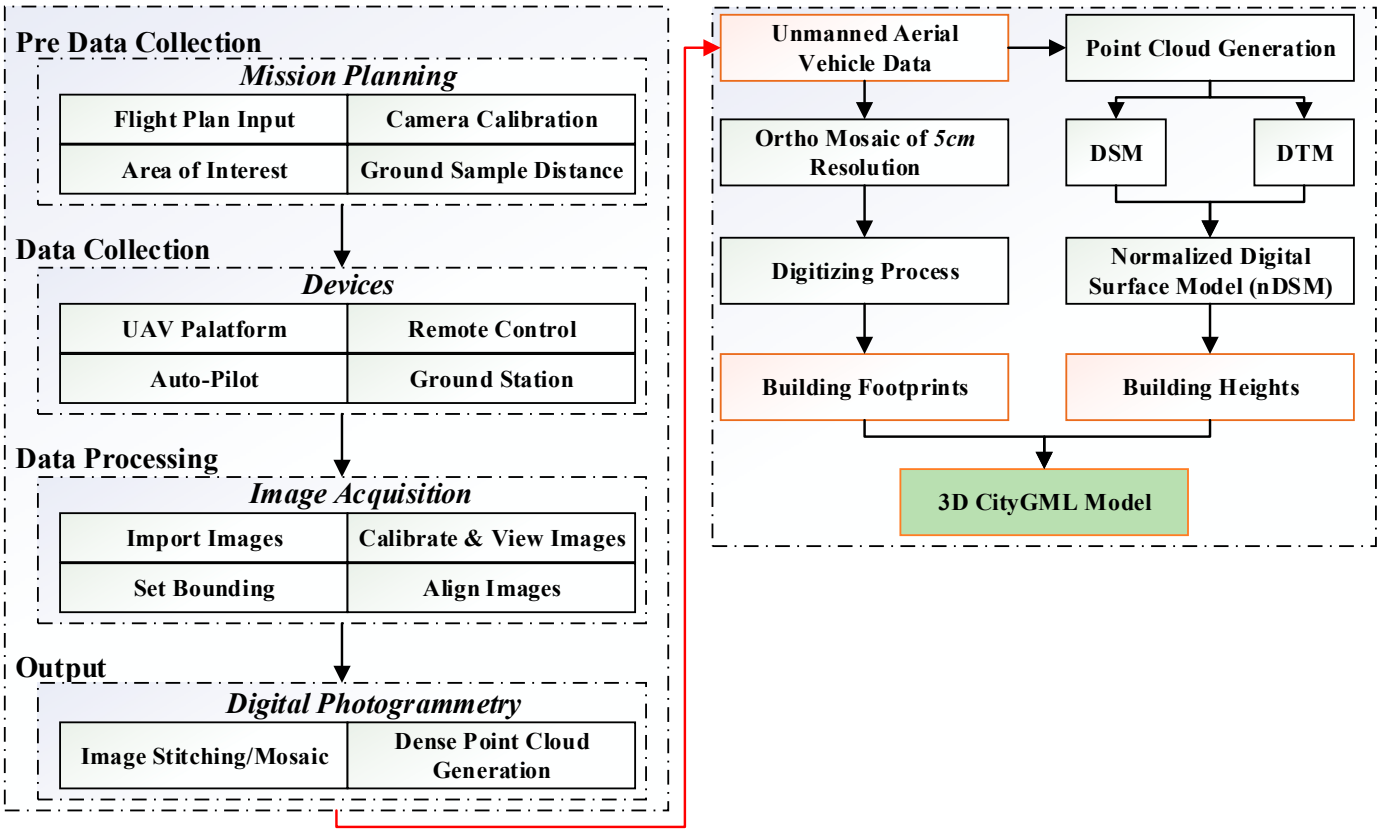

Figure 3. Working methodology to generate a 3D city model from the UAV dataset.

3. Construction of 3D City Model

Three-dimensional city modeling can facilitate urban planning, property development, better transportation, disaster simulation, tourism development, sustainable environmental development, social and economic analysis, architecture and design, etc. [38]. The DEM Point Cloud data derived from the UAV survey were processed in Global Mapper software to transform raw data to obtain the Digital Surface Model (DSM) and Digital Terrain Model (DTM). DSM is a depiction of the environment's native and artificial elements, such as trees, buildings, and other structural elements, which exist within the topographic surface of the bare earth's surface. In contrast to DSM, which also includes all static features like vegetation, cars, and buildings, a DTM only shows the land's surface [16]. The DTM point cloud having the RGB colors associated with the terrain height is shown in Figure 4a and the DSM point cloud capturing all the features in the study area is shown in Figure 4b. A Normalized Digital Surface Model (nDSM) is calculated by subtracting DTM from DSM. The Orthomosaic derived from UAV was used to extract building footprints, as shown in Figure 5. Using the centroids of each building footprint and nDSM, the corresponding height information of each building footprint is extracted [39].

A simplified three-dimensional city model with LoD-1 is generated by extruding building footprints with the obtained height of each building by following the methodology shown in Figure 3. The Open Geospatial Consortium (OGC) released CityGML [40], a standardized data model in XML format. The format of the 3D models of city and landscape characteristics might be exchanged between various applications and platforms due to this standardized data model. Mapping, environment, urban planning, real estate, navigation, simulation, architecture, and urban facilities management are just a few of the areas in which these interchangeable formats can be used. The generated city model was imported to MATLAB and visualized, as it offers a wide range of tools and functions for data visualization [34]. Figure 6 showcases the digital representation of constructed buildings in the study area. The ground survey was conducted to validate the obtained building

attributes; vertical and horizontal accuracy was found to be ±0.2 m and ±0.3 m, respectively.

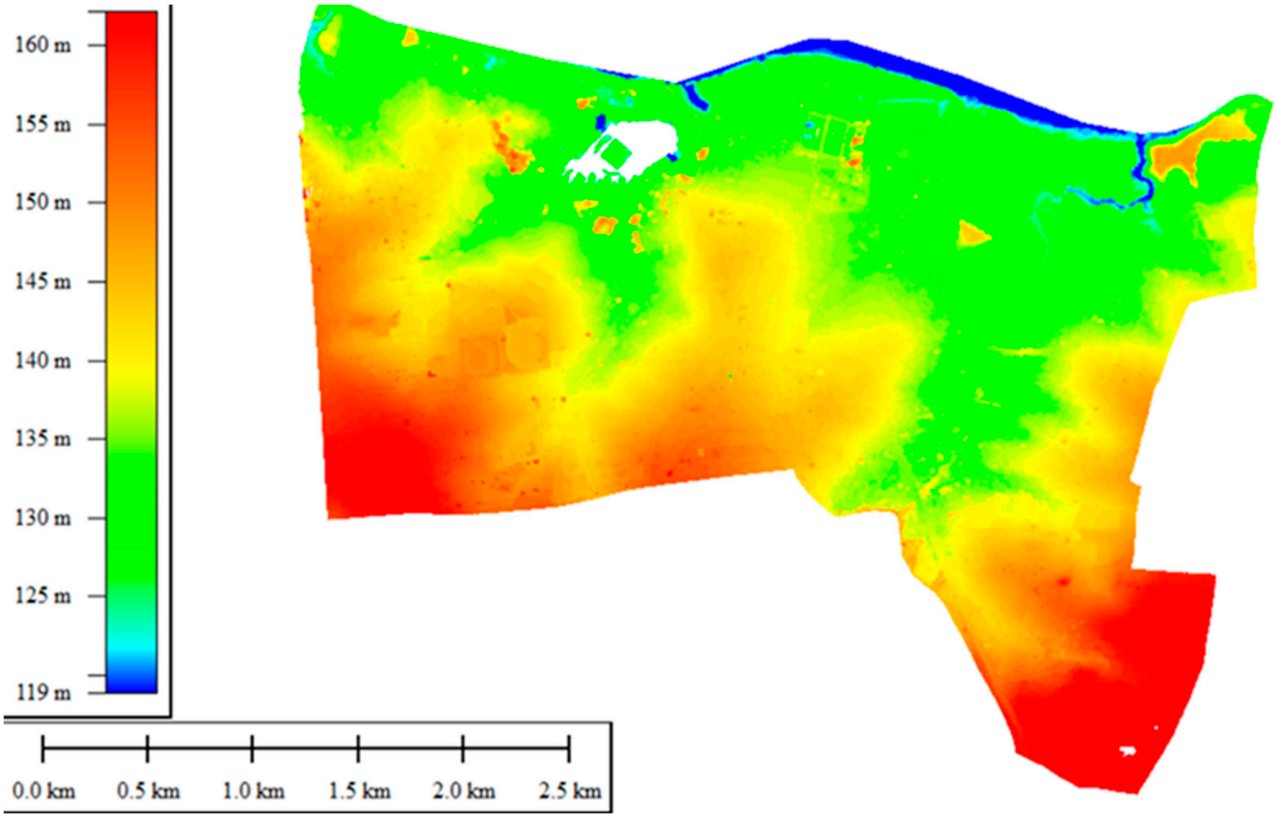

(**a**)

(**b**)

Figure 4. Digital surface models. (**a**) DTM RGB point cloud data showing the terrain elevation information. (**b**) The DSM point dense cloud shows all the features of the study area.

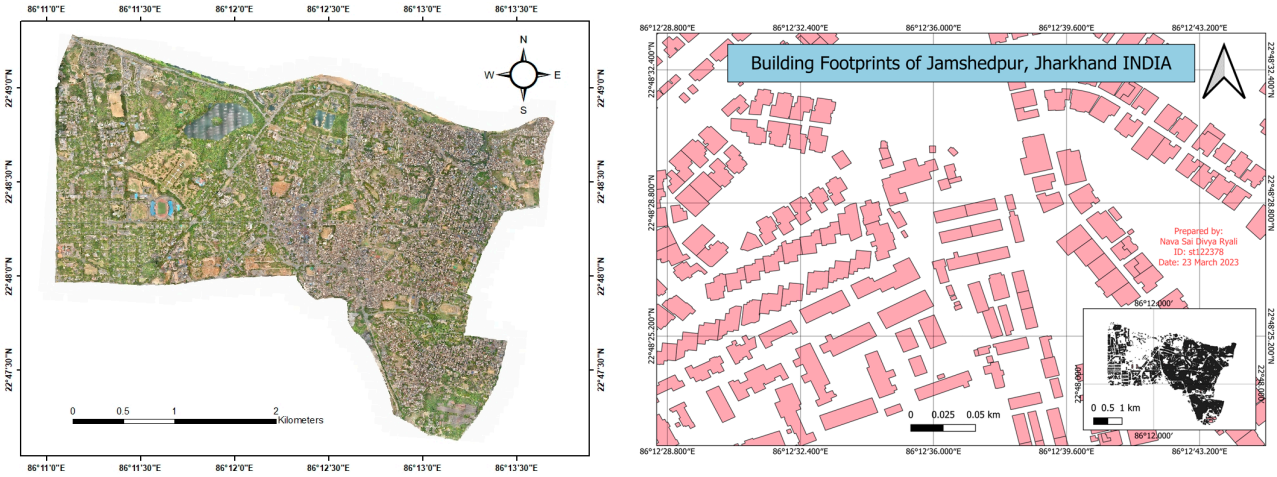

(**a**) (**b**)

Figure 5. UAV aerial imaging and mapping. (**a**) Ortho Mosaic of the study area. (**b**) Map showing the extracted footprints of the study area.

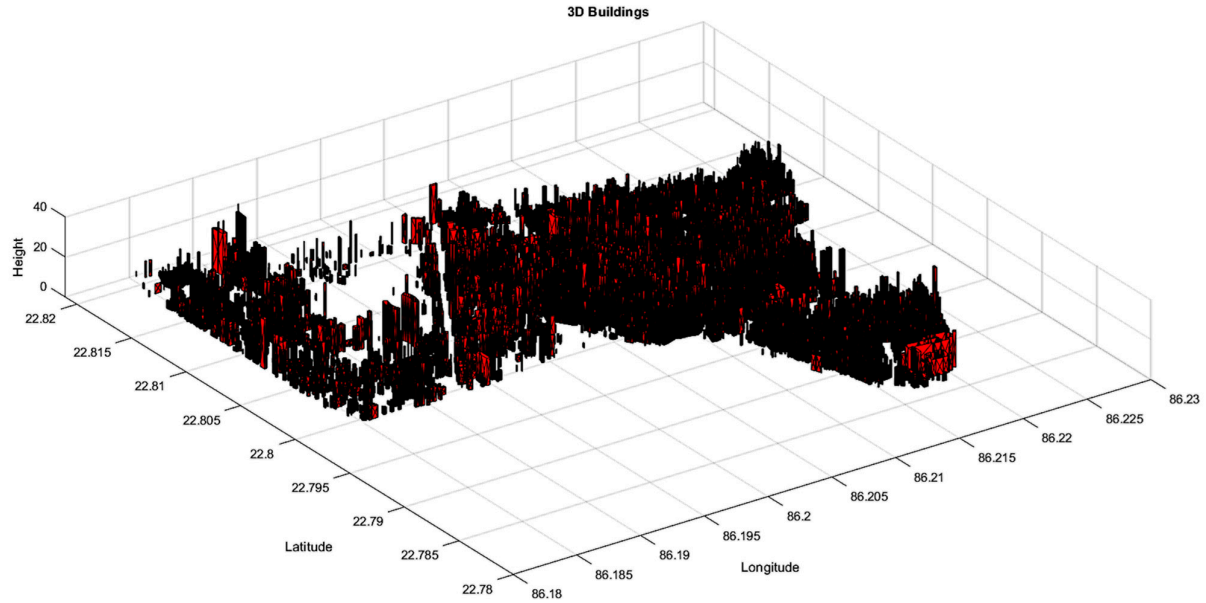

(**a**)

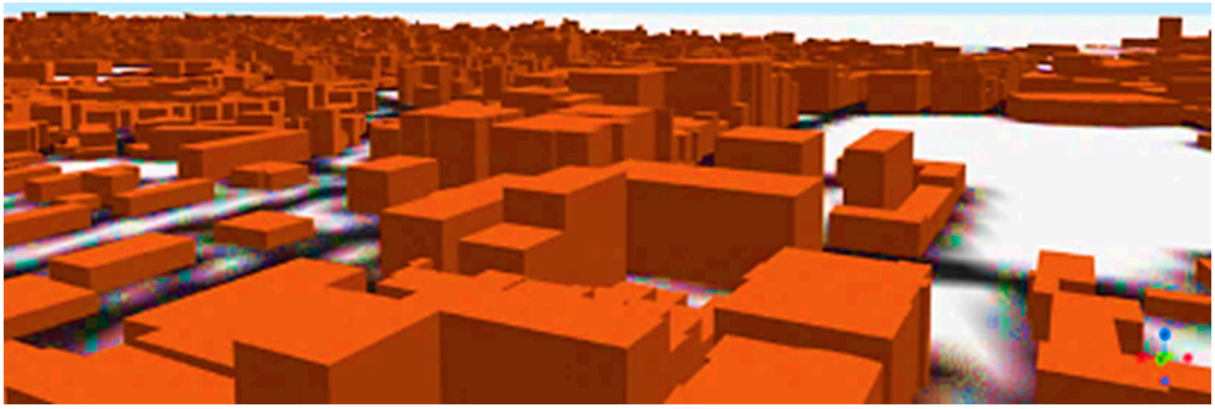

(**b**)

Figure 6. MATLAB-based virtual urban data visualization. (**a**) Three-dimensional city model of study area. (**b**) Close-up view of 3D city model to showcase the level of detail 1.1 on the set of buildings.

Building Dataset

Building dataset attributes are classified using MATLAB to understand the physical factors contributing to building energy performances and help gain insights into the relationships between building attributes and incoming solar irradiation. The attributes are assigned for each building in the dataset. Building attributes like building IDs, geometry statistics like the height of the building, rooftop areas, wall areas, and building parcel directions are made concisely in the master dataset, which is essential to obtain accurate solar radiation. The statistical analysis to classify building features will assist in conducting a correlation analysis between building entities and solar potential. The distribution map of building heights, rooftop area, and facade area for the selected region under study are shown in Figure 7. The area surveyed is 9.7 km^2, having 30978 buildings with a rooftop area of 2.67 km^2 and a facade area of 6.79 km^2. After eliminating buildings less than 2.5 m in height and with a footprint area of less than 20 m^2, the building height was validated with field observations, and the maximum height of the building was 37.7 m.

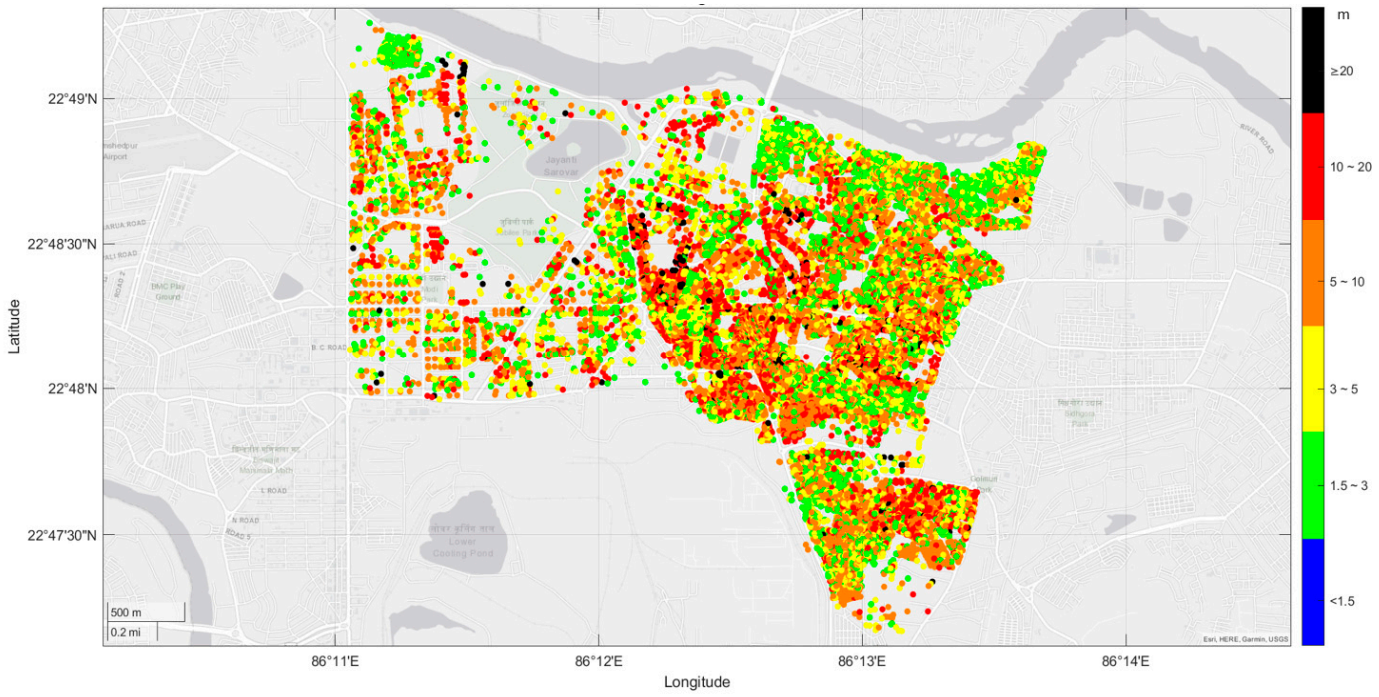

(**a**)

Figure 7. *Cont.*

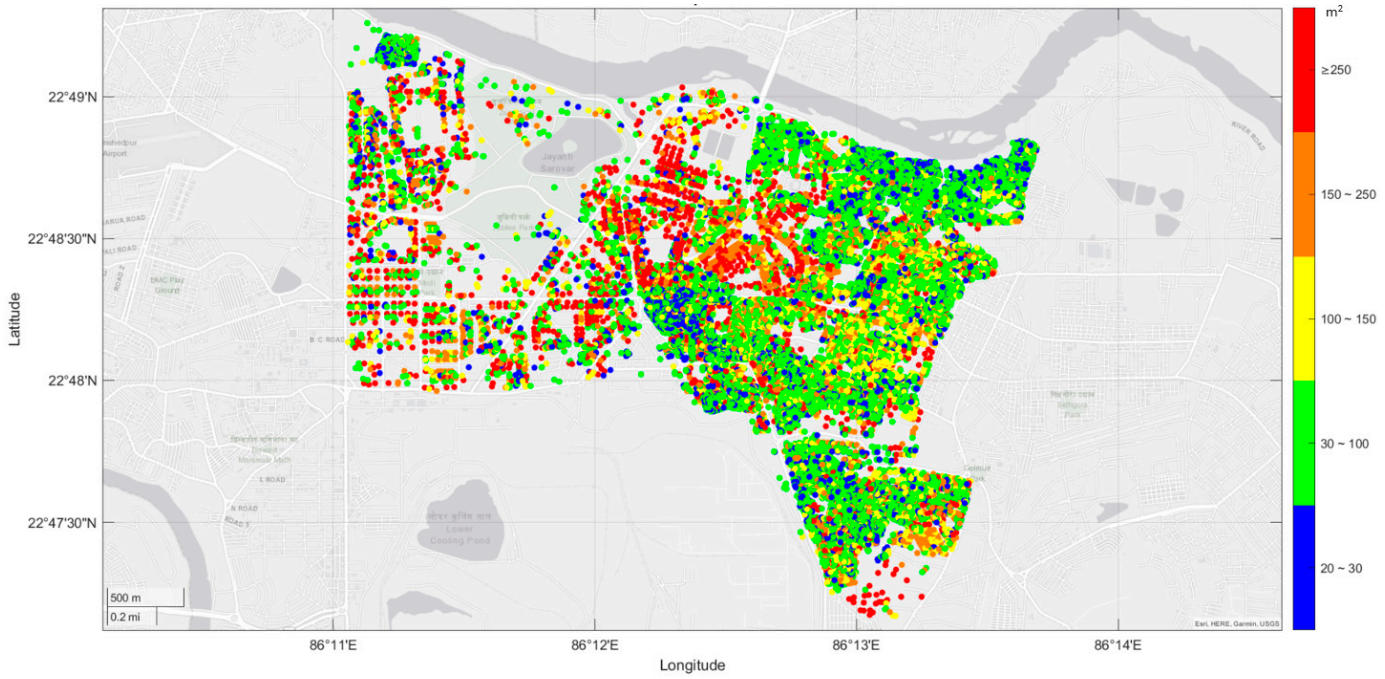

(**b**)

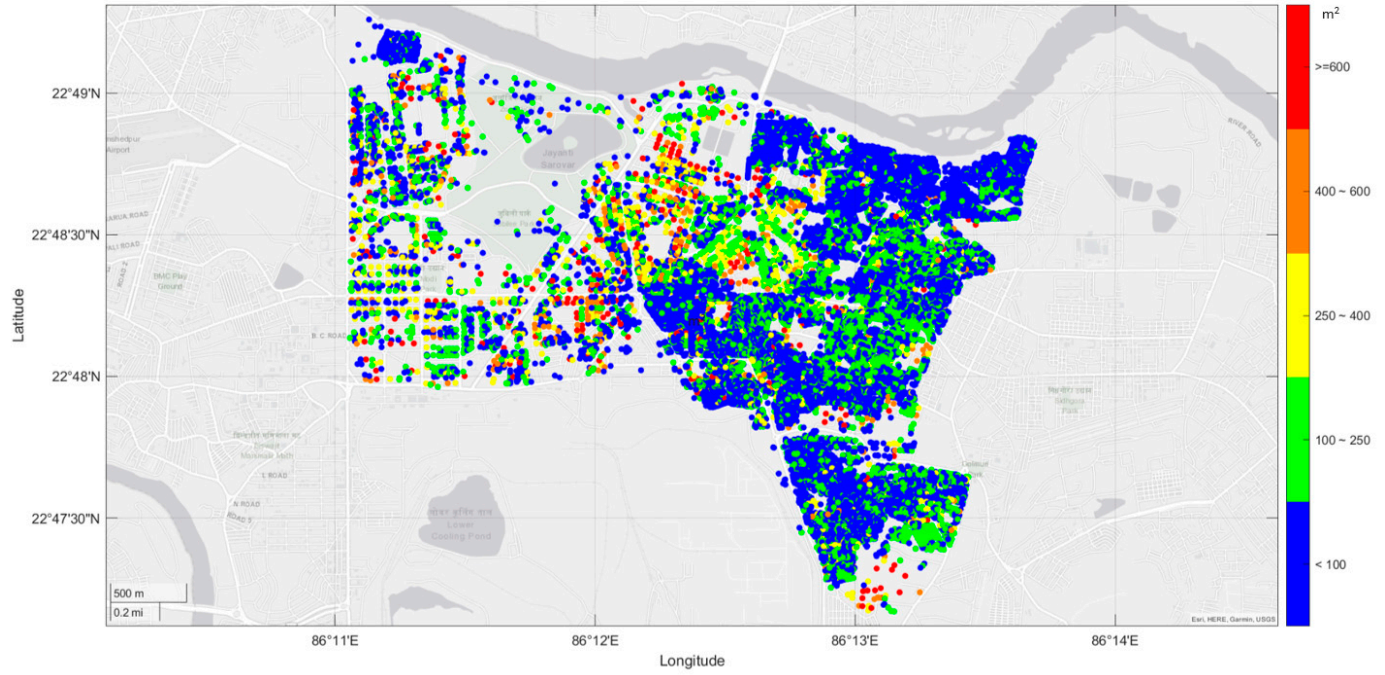

(**c**)

Figure 7. Map view of classified building attributes in MATLAB. (**a**) Building height classification. (**b**) Building rooftop area classification. (**c**) Building facade area classification.

4. Solar Radiation Calculation

Geospatial modelling is carried out using MATLAB Mapping toolbox to estimate the theoretical solar radiation attained by the building envelopes; the effects of time-varying shading events are counted to enhance the estimation of direct irradiance and diffuse radiation by considering turbidity factors depending on atmospheric conditions [41], as shown in Figure 8. MATLAB software is a powerful numerical analysis program widely

used in the research community for energy modelling and solar analysis [42–44]. Mapping tools are proficient in generating high-quality graphical displays of geospatial data. The toolbox provides functions and user interfaces to import, create, manipulate, simulate, and represent geospatial data [45–47].

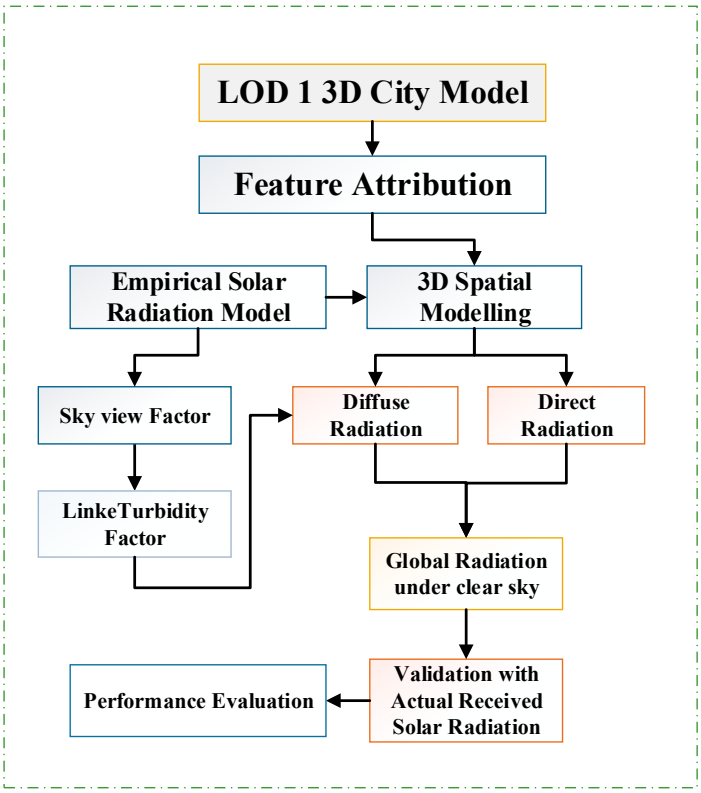

Figure 8. Geospatial modelling framework for obtaining solar potential.

The irradiance accumulates over time and in different areas to represent the total irradiance that can be theoretically received by each wall, roof, and building during each day, month, or year. Ghouard's model proposed empirical formulas related to astronomical parameters and atmospheric conditions [48] that estimate solar radiation in the region according to the latitudes.

The hourly global irradiance $\left(E_{global}\right)$ for the sunshine duration throughout the year has been calculated for all the building surfaces in the study area and is obtained using Equation (1), as shown below:

$$E_{global}(h) = E_{direct} + E_{diffuse} \tag{1}$$

where:

- h is the sunshine hours.
- E_{direct} is the irradiance directly incident on a face per unit area and can be calculated using Equation (2), as shown below:

$$E_{direct} = S_o C_t A_1 \exp\left(-\frac{A_2}{\sin(h_s)}\right)\sin(h_s) \tag{2}$$

C_t is the correction factor for earth–sun distance, which varies from 144 (21 December) to 154 million km (21 June) and can be calculated using Equation (3), as shown below:

$$C_t = 1 + 0.034\cos(j-2),\ j \in [1,\ 365] \tag{3}$$

- j is the day number of the year, ranging from 1 on 1 January to 365 on 31 December;

- S_o is the solar constant, which is defined as the energy flux received per unit area having a value of 1367 W/m^2;
- A_1 and A_2 are coefficients of the turbidity factor;
- h_s is solar elevation in degrees, representing the angle between the horizontal plane with the sun direction, which varies from −90 (nadir) to 0 at sunrise and sunset to −90 (zenith) and is calculated using Equation (4) from the geographical coordinates represented by the latitude (ϕ *degrees*), solar declination (δ *degrees*), and altitude hour angle (ω *degrees*), as shown below:

$$\sin(h_s) = \sin(\phi)\sin(\delta) + \cos(\phi)\cos(\delta)\cos(\omega) \quad (4)$$

- $E_{diffuse}$ is the diffuse irradiance that comes from all the space and has no privileged orientation and is calculated using Equation (5), as shown below:

$$E_{diffuse} = S_o C_t \left(0.271 - 0.2939 A_1 \exp\left(-\frac{A_2}{\cos(h_s)}\right)\right)\cos(h_s) \quad (5)$$

5. Results

PV modules are preferred for installation in areas with high spatial concentrations of solar radiation. The annual solar radiation for each building surface is simulated based on the accumulation of hourly solar irradiation over 2023. Vast areas of building surfaces, including rooftops and walls, will receive solar radiation in the region. The global irradiation for all the building envelopes is computed hourly; the duration in shadow for each building envelope is counted to exclude the proportion of solar irradiation. The surrounding buildings are recognized for shadow tracing for each building, as shown in Figure 9. The solar elevation, azimuth, and incidence angle were calculated hourly, which is crucial for shadow tracing. For the selected building rooftop, if the surrounding building altitudes are lower, no shadow will be cast on the rooftop. The selected building facades' relative altitude is calculated, and the shading relationship is framed based on the geographical coordinates, building geometry, surface azimuth, solar azimuth, and tilt angle. The developed model calculates solar irradiation on an hourly basis during sunshine hours. Hence, the daily, monthly, or yearly average radiation can be estimated on selected buildings and building envelopes. The distribution of solar irradiation on facades is simulated by considering the building wall azimuth, and the tilt is assumed to be 90 degrees.

Figure 10 shows the visual representation of average solar irradiation for the selected month and year on a set of sample building rooftops. The developed model can accumulate the solar irradiance received by any surface of the building or set of selected buildings during any day, month, or year. The 3D map outputs showcasing the solar potential can be simulated for the preferred location and time, as shown in Figure 11. Also, ground measurements are performed using a pyranometer to measure global irradiance on the sample building rooftop hourly throughout 2023 to validate the model performance on rooftop solar potential. The experimental setup consists of a pyranometer to measure the solar radiation, a web camera was adjusted to read the solar radiation from the pyranometer display, and the laptop recorded the video feed from the webcam, as shown in Figure 12.

The hourly solar irradiation is accumulated for the year, and the distribution of monthly average global solar irradiation of the building surfaces in the study area, which is classified based on building surface orientation, is shown in Figure 13. The visual representation of the distribution analysis provides valuable insights into how solar energy potential varies depending on the orientation of the rooftops and facades. This level of detail enables decision-makers to identify the optimal surface orientations for the specific geographical location that maximizes solar energy generation throughout the year. Solar radiation had almost even distribution in the west and east direction facades. North facades received barely minimum irradiation, and shadowing events affected most west-direction facades.

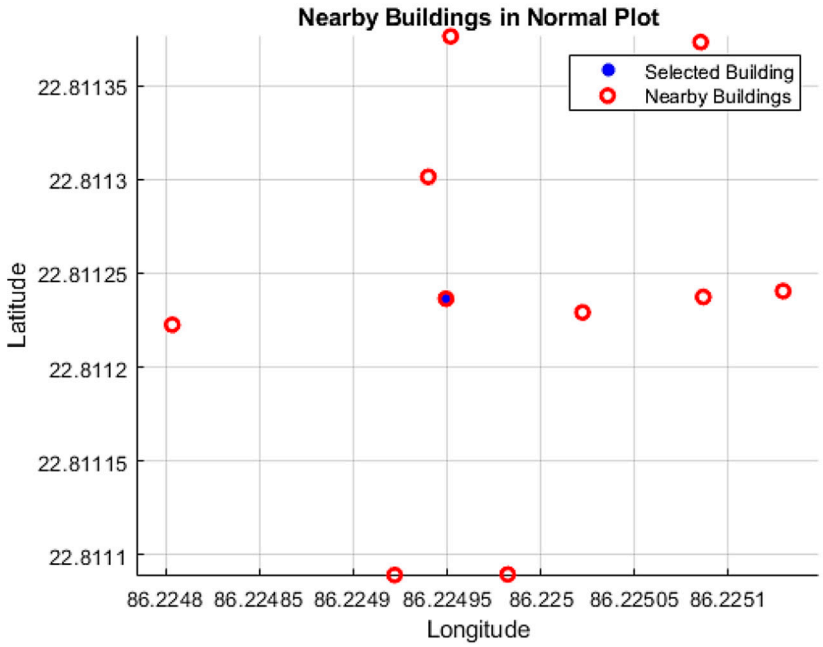

Figure 9. Selection of nearby buildings for shadow castings in the normal plot.

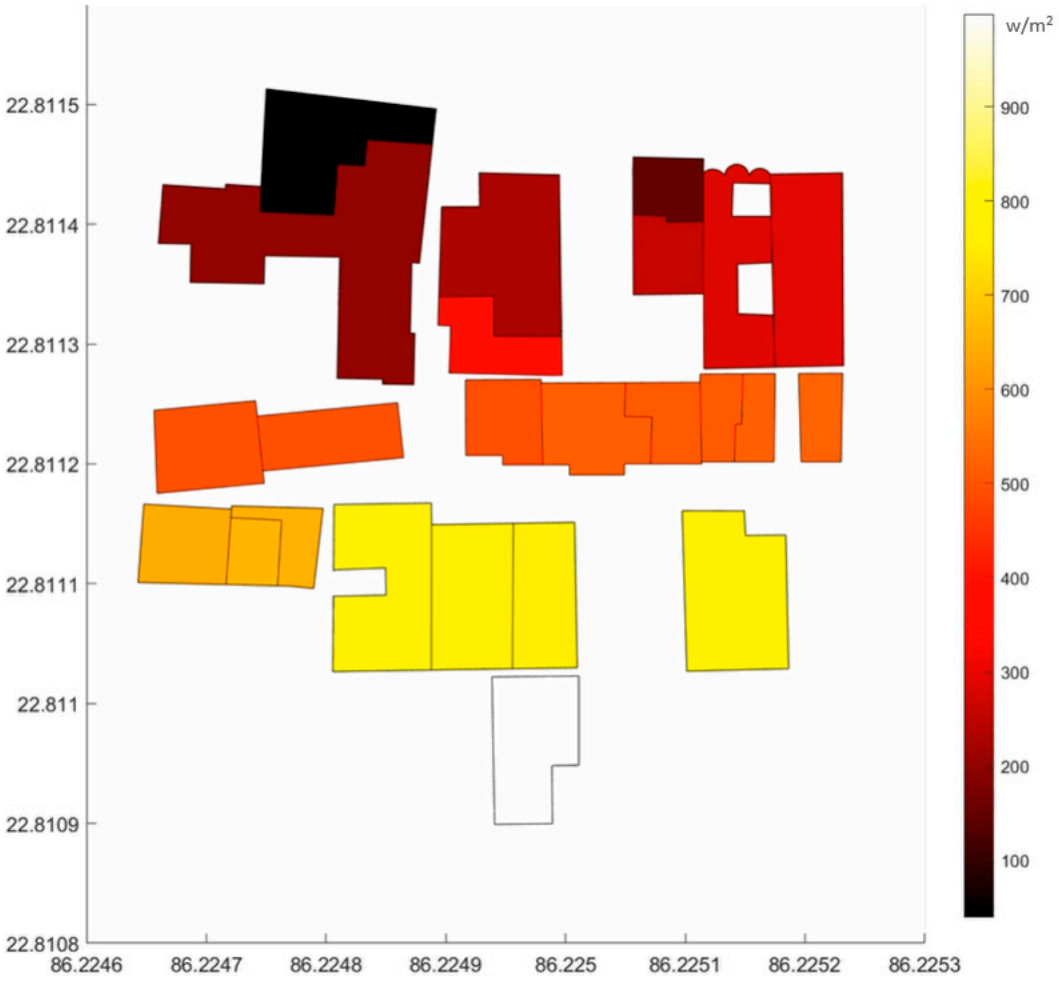

Figure 10. Two-dimensional map view of average daily solar irradiance on a set of building rooftops in the study area for March 2023.

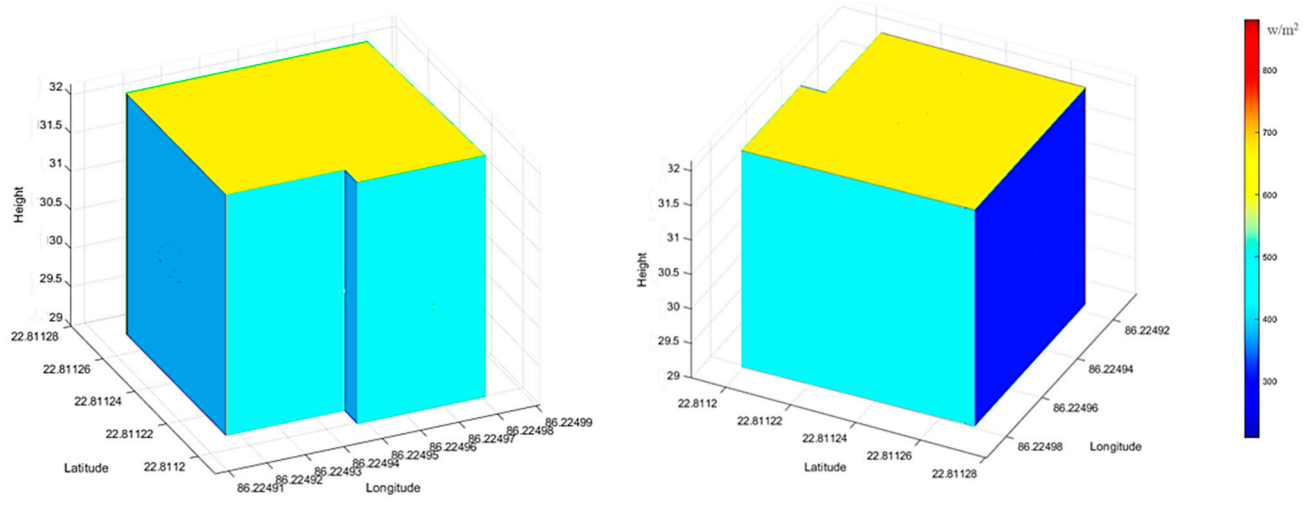

(**a**)

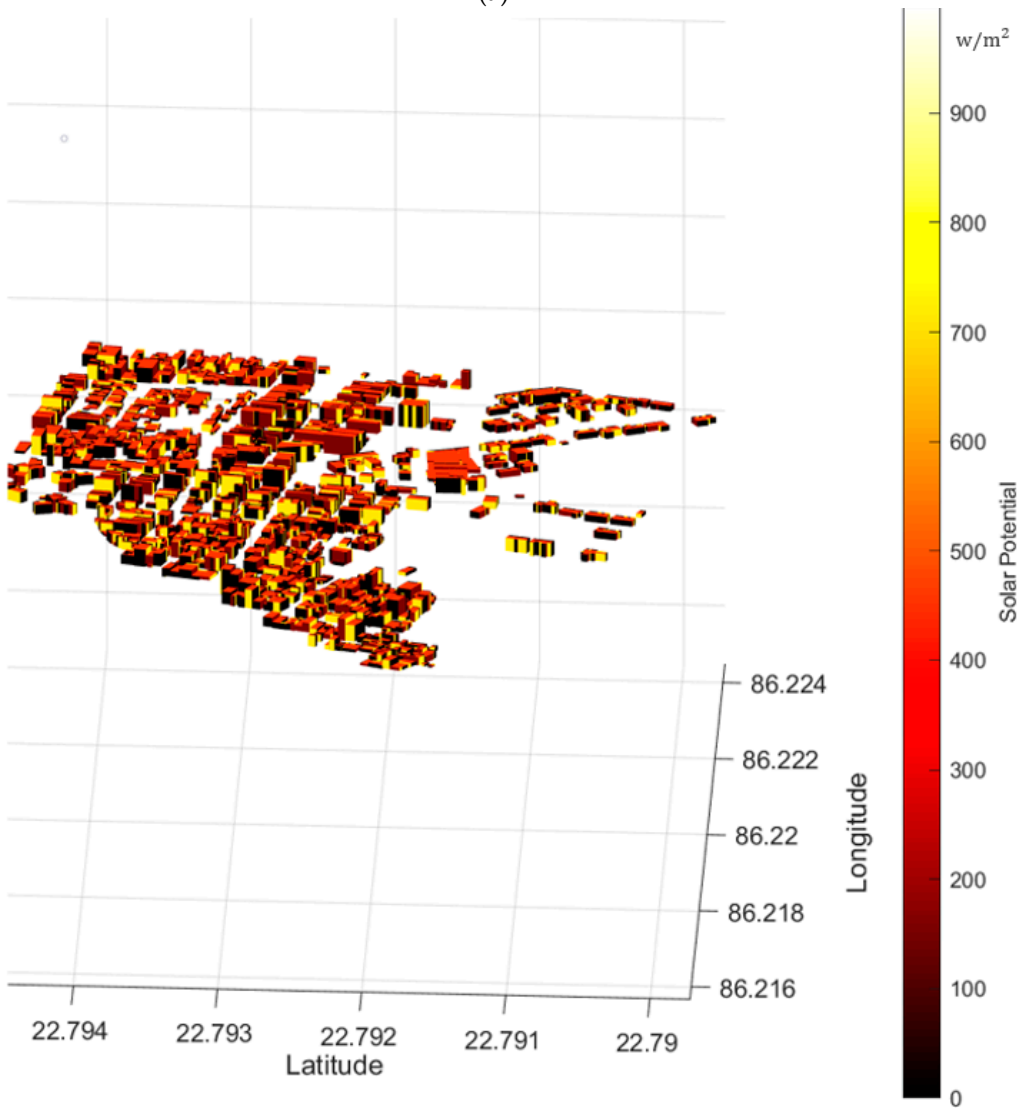

(**b**)

Figure 11. Simulation outputs of solar radiation on building envelopes. (**a**) Three-dimensional map view of solar radiation on single selected building at 11 a.m. on 22 February 2023. (**b**) Three-dimensional map view of solar potential on set of building at 8 a.m. on 1 June 2023.

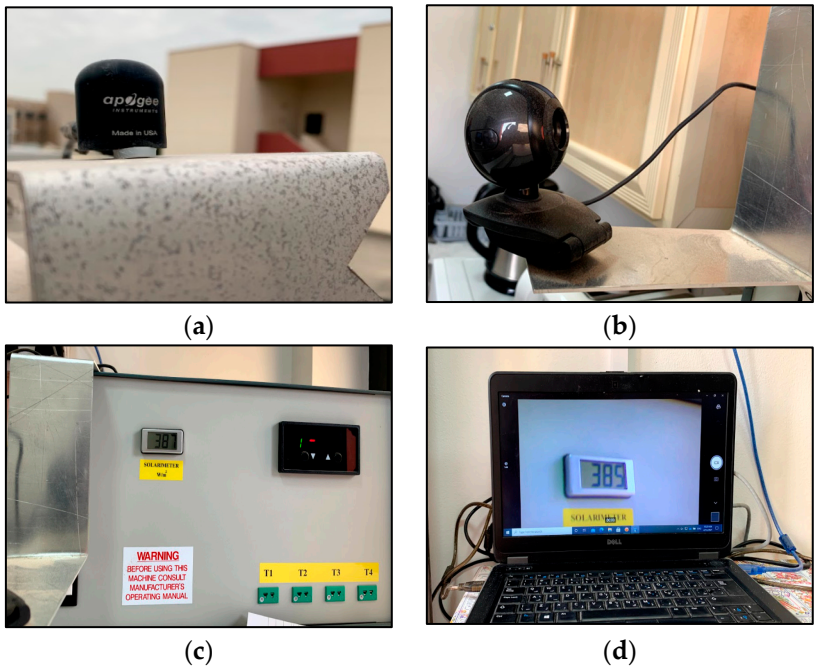

Figure 12. An experimental setup will be used to record the actual solar irradiance of the region. (**a**) Pyranometer. (**b**) Webcam. (**c**) Pyranometer reading. (**d**) Laptop.

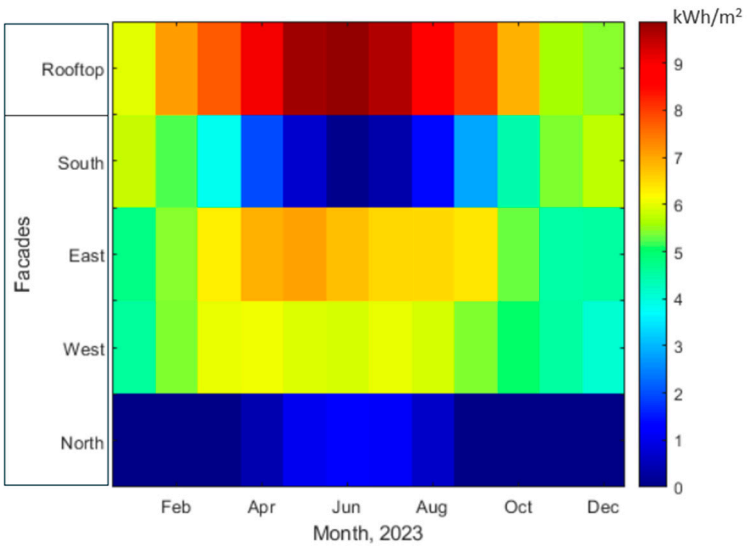

Figure 13. Computed average monthly global solar irradiation on rooftops and facades.

The monthly average daily irradiation values (GHI) for the study area range from 3.87 kWh/m^2 (December) to 9.23 kWh/m^2 (May). The monthly average solar irradiation onsite for the selected rooftop (Figure 12) is 7.0366 kWh/m^2, while the simulated value is 7.358 kWh/m^2. This reveals that the strong correlation coefficient between simulated and actual irradiation values is R = 0.83.

The PV yield is computed for the study area, and the effective area for deploying solar PV systems on the building surface is assumed to be 50% [27]. Annual solar potential of 310.149 TWh is estimated for the research region and the monthly distribution of estimated PV energy supply on building surfaces is shown in Figure 14. This detail is crucial for optimizing the placement of solar PV systems to maximize renewable energy production from the available building surfaces.

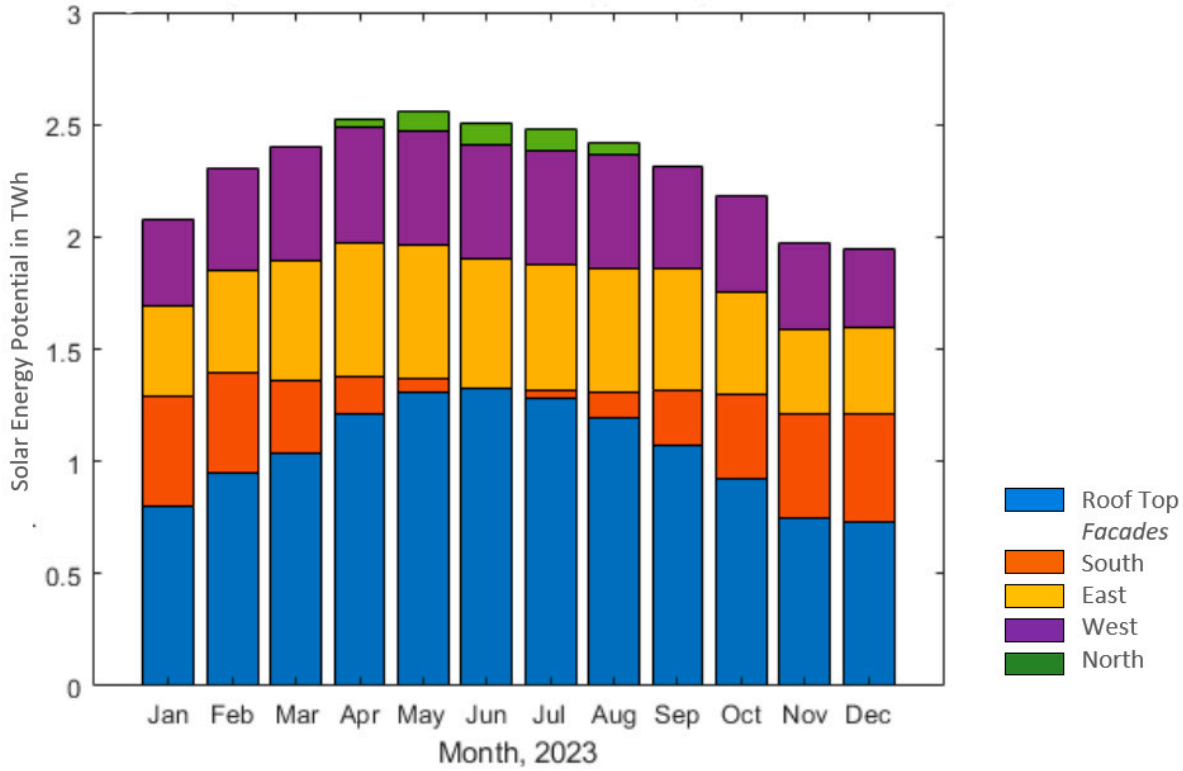

Figure 14. Computed solar PV generation of building surfaces in the study area.

Urban building forms (UBFs) can impact the solar potential. Two UBF indicators (surface area and building height) are chosen to compute their relationship with urban solar potential [49]. The relationship between these two indicators with solar potential is explored by creating scatter plots. In the correlation analysis, the coefficient of determination between building rooftop area and solar potential was $R^2 = 0.89$, and between building heights and incoming solar potential, it was $R^2 = 0.354$. The results indicate that the surface area is directly proportional to the solar potential, and building height alone is not a feasible indicator.

6. Implications and Limitations

The developed model proposed an effective solution to construct a simplified 3D solar city map by integrating building facades along with the rooftops. The generated 3D city model is based on the CityGML standard, which utilizes Geographic Markup Language (GML). It is an object-oriented data model that helps in generating 3D vector data. In recent years, planning of smart cities has taken a new trend involving 3D modelling using CityGML, as it is an open data model for storage, analysis, and representation, and it facilitates the interoperability of virtual 3D city models.

The framework to assess solar potential can be applied to any CityGML-based city model with Level of Detail-1 as the input data sources, processing algorithms, and visualization components, which can be tailored to the specific characteristics. Using the geometric information available in the CityGML dataset, the Ghouard-based empirical model can assess the solar incidence angles on building surfaces based on the sun path for any location.

The code can be customized based on the various input parameters for the selected location, like longitude correction, solar declination, solar azimuth, elevation, zenith, sun-earth distance correction factor, turbidity factors based on atmospheric conditions, climate data, etc. The findings are specific to the study region and might not be directly applicable to other urban areas without adjustments for local conditions. However, the

code developed for this model can be customized to adapt to other urban contexts beyond the case study presented.

It is a challenge to obtain detailed building models in large urban areas; the generated city model with Level of Detail-1 assumes that the rooftops are all flat. The received solar radiation is significantly affected by sky clearness (cloudy, sunny, rainy) and atmospheric air turbidity. This study calculates solar irradiance by assuming that clear sky and air turbidity are normal. The diffuse radiation is anisotropic hourly radiation, whereas the urban atmosphere is complicated and all the elements in the urban system will absorb and generate radiation, which will affect the radiation attained by the buildings. The albedos of materials used in building surfaces will also impact the solar radiation received by the building surfaces, which is not considered part of the model.

The study uses simplified geometrical details for buildings, which might not accurately capture complex shading patterns. This could lead to less precise simulations of solar potential. The model does not consider other important UBF indicators such as terrain variations, vegetation/green cover, materials, road networks, built density, and surface-to-volume ratio. Including these factors could provide a more comprehensive analysis. The current model is a scripted code, which limits its accessibility for end users who may not have the technical expertise to use it effectively. Despite the limitation, the model can assist in renewable energy integration and urban planning. The study highlights the impact of facade orientation but does not provide detailed guidelines or solutions for optimizing building designs to maximize solar potential across different orientations. The analysis shows significant shading losses but does not explore potential mitigation strategies for these buildings.

7. Conclusions

This study proposed a simplified 3D solar city model by integrating unmanned aerial vehicle (UAV) datasets into MATLAB by acquiring geographic data to conduct spatial analysis to simulate the solar potential on building envelopes, considering the shadowing effects. The study and investigation of solar irradiation in relation to building parameters is essential to identify the practical solar potential of any urban built form. Urban areas are limited in available space, so harnessing the solar radiation from building facades could be effective if significant portions receiving solar radiation are utilized. The findings in the study show that shading effects have impacted the incoming solar irradiation, especially on facades, to increase the solar capacity.

The building rooftops and facades receive an estimated global irradiance of 1323.95 kWh/m^2/year and 821.65 kWh/m^2/year, respectively, in the study region. The impact of façade orientation is evident, as north-facing facades received only 1% of total solar distribution on building surfaces. The rooftops less than 5m in height are dramatically losing almost 46% of direct solar radiation due to shading events. Potential mitigation strategies can be explored in future research. The buildings in the region are categorized based on the received solar irradiation; almost 4405 buildings receive higher than 10 GWh/year, and 8089 buildings receive between 5.0 and 10 GWh/year. The impact of shading loss is significant, as the study area is densely populated. The rooftops of high-rise buildings are not affected by shading, thereby being potential places for PV installations.

The findings illustrate physical constraints of urban built forms and morphology, e.g., building surface area, orientation, and associated building heights can significantly affect the incoming solar radiation, highlighting the necessity to consider urban built forms for sustainable urban planning and development.

Previous methodological approaches to rooftop solar assessments use multiple software, technologies, tools, and models [16,27]. MATLAB Mapping toolbox, used as a simulation tool in this study, leverages a single platform to conduct solar potential analysis on building surfaces and continues with the correlation analysis of UBF indicators with solar potential. The unified approach enhances the feasibility and cost-effectiveness, facil-

itating comprehensive exploration of the relationship between UBF indicators and solar energy potential.

Author Contributions: N.S.D.R. conceptualized the study, analyzed the data, interpreted the results, and wrote the manuscript. N.K.T. guided the development of the research idea and supervised the research. S.N. and J.G.S. provided suggestions and comments on the research idea. N.K.T. and J.G.S. supervised the revision process to address the reviewer's comments. All authors have read and agreed to the published version of the manuscript.

Funding: This research received no external funding.

Data Availability Statement: Data supporting the findings of this study are available from the corresponding author on request.

Acknowledgments: We would like to acknowledge VR Map Creators Pvt Ltd. (VRMC) for assisting in conducting a UAV survey in December 2022.

Conflicts of Interest: The authors declare no conflict of interest.

References

1. Sawhney, A. Striving towards a circular economy: Climate policy and renewable energy in India. *Clean Technol. Environ. Policy* **2021**, *23*, 491–499. [CrossRef]
2. Liu, H.; Khan, I.; Zakari, A.; Alharthi, M. Roles of trilemma in the world energy sector and transition towards sustainable energy: A study of economic growth and the environment. *Energy Policy* **2022**, *170*, 113238. [CrossRef]
3. Kumar, C.M.S.; Singh, S.; Gupta, M.K.; Nimdeo, Y.M.; Raushan, R.; Deorankar, A.V.; Kumar, T.A.; Rout, P.K.; Chanotiya, C.; Pakhale, V.D.; et al. Solar energy: A promising renewable source for meeting energy demand in Indian agriculture applications. In *Sustainable Energy Technologies and Assessments*; Elsevier Ltd.: Amsterdam, The Netherlands, 2023; Volume 55. [CrossRef]
4. Kumar, R.; Kumar, A.; Gupta, M.K.; Yadav, J.; Jain, A. Solar tree-based water pumping for assured irrigation in sustainable Indian agriculture environment. *Sustain. Prod. Consum.* **2022**, *33*, 15–27. [CrossRef]
5. Ministry of New and Renewable Energy, Government of India. *Annual Report 2022–2023*; Ministry of New and Renewable Energy, Government of India: New Delhi, India, 2023.
6. Deb, S.; Okulicz-Kozaryn, A. Exploring the association of urbanisation and subjective well-being in India. *Cities* **2023**, *132*, 104068. [CrossRef]
7. Biswas, M.A.R.; Robinson, M.D.; Fumo, N. Prediction of residential building energy consumption: A neural network approach. *Energy* **2016**, *117*, 84–92. [CrossRef]
8. Gujar, S.; Deshmukh, A.; Chivate, A. The role of open-built space morphology in residential environment quality assessment of cluster housing. *METU J. Fac. Archit.* **2022**, *39*, 181–200. [CrossRef]
9. Kaleshwarwar, A.; Bahadure, S. Validating the credibility of solar simulation tools using a real-world case study. *Energy Build.* **2023**, *301*, 113697. [CrossRef]
10. Salleh, S.; Ujang, U. Topological information extraction from buildings in CityGML. In Proceedings of the IOP Conference Series: Earth and Environmental Science, Kuala Lumpur, Malaysia, 24–25 April 2018; Institute of Physics Publishing: Bristol, UK, 2018. [CrossRef]
11. Pan, Y.; Zhu, M.; Lv, Y.; Huang, S. Building energy simulation and its application for building performance optimization: A review of methods, tools, and case studies. *Adv. Appl. Energy* **2023**, *10*, 100135. [CrossRef]
12. Bartmiński, P.; Siłuch, M.; Kociuba, W. The Effectiveness of a UAV-Based LiDAR Survey to Develop Digital Terrain Models and Topographic Texture Analyses. *Sensors* **2023**, *23*, 6415. [CrossRef]
13. Kaartinen, E.; Dunphy, K.; Sadhu, A. LiDAR-Based Structural Health Monitoring: Applications in Civil Infrastructure Systems. *Sensors* **2022**, *22*, 4610. [CrossRef]
14. Casella, E.; Drechsel, J.; Winter, C.; Benninghoff, M.; Rovere, A. Accuracy of sand beach topography surveying by drones and photogrammetry. *Geo-Mar. Lett.* **2020**, *40*, 255–268. [CrossRef]
15. Le Van, C.; Cao, C.X.; Nguyen, A.N.; Van Pham, C.; Nguyen, L.Q. Building 3D CityGML models of mining industrial structures using integrated UAV and TLS point clouds. *Int. J. Coal Sci. Technol.* **2023**, *10*, 69. [CrossRef]
16. Jain, K.; Khoshelham, K.; Zhu, X.; Tiwari, A. Lecture Notes in Civil Engineering Unmanned Aerial System in Geomatics, Proceedings of UASG 2019. Available online: http://www.springer.com/series/15087 (accessed on 7 April 2019).
17. Bangkui, F.; Yun, L.; Ruiyu, Z.; Qiqi, F. Review on the technological development and application of uav systems. *Chin. J. Electron.* **2020**, *29*, 199–207. [CrossRef]
18. Djenaliev, A.; Chymyrov, A.; Kada, M.; Hellwich, O.; Akmatov, T.; Golev, O.; Chymyrova, S. Unmanned Aerial Systems for Building Footprint Extraction in Urban Area. *Int. J. Geoinform.* **2024**, *20*, 64–81. [CrossRef]
19. Borràs, I.M.; Neves, D.; Gomes, R. Using urban building energy modeling data to assess energy communities' potential. *Energy Build.* **2023**, *282*, 112791. [CrossRef]

20. Cao, X.; Dai, X.; Liu, J. Building energy-consumption status worldwide and the state-of-the-art technologies for zero-energy buildings during the past decade. *Energy Build.* **2016**, *128*, 198–213. [CrossRef]
21. Sun, T.; Shan, M.; Rong, X.; Yang, X. Estimating the spatial distribution of solar photovoltaic power generation potential on different types of rural rooftops using a deep learning network applied to satellite images. *Appl. Energy* **2022**, *315*, 119025. [CrossRef]
22. Chen, Z.; Yu, B.; Li, Y.; Wu, Q.; Wu, B.; Huang, Y.; Wu, S.; Yu, S.; Mao, W.; Zhao, F.; et al. Assessing the potential and utilization of solar energy at the building-scale in Shanghai. *Sustain. Cities Soc.* **2022**, *82*, 103917. [CrossRef]
23. Simsek, Y.; Watts, D.; Escobar, R. Sustainability evaluation of Concentrated Solar Power (CSP) projects under Clean Development Mechanism (CDM) by using Multi Criteria Decision Method (MCDM). *Renew. Sustain. Energy Rev.* **2018**, *93*, 421–438. [CrossRef]
24. Calcabrini, A.; Weegink, R.; Manganiello, P.; Zeman, M.; Isabella, O. Simulation study of the electrical yield of various PV module topologies in partially shaded urban scenarios. *Sol. Energy* **2021**, *225*, 726–733. [CrossRef]
25. Han, J.Y.; Chen, Y.C.; Li, S.Y. Utilising high-fidelity 3D building model for analysing the rooftop solar photovoltaic potential in urban areas. *Sol. Energy* **2022**, *235*, 187–199. [CrossRef]
26. Gonçalves, R.S.; Palmero-Marrero, A.I.; Oliveira, A.C. Educational solar energy tool in Matlab environment. *Energy Rep.* **2020**, *6*, 490–495. [CrossRef]
27. Kaleshwarwar, A.; Bahadure, S. Assessment of the solar energy potential of diverse urban built forms in Nagpur, India. *Sustain. Cities Soc.* **2023**, *96*, 104681. [CrossRef]
28. Batakanwa, N.C. Validating Uav-Sfm Photogrammetry Heights for Highway Topographic Surveying in Tanzania. *S. Afr. J. Geomat.* **2024**, *13*, 38–50.
29. Messaoudi, K.; Oubbati, O.S.; Rachedi, A.; Lakas, A.; Bendouma, T.; Chaib, N. A survey of UAV-based data collection: Challenges, solutions and future perspectives. *J. Netw. Comput. Appl.* **2023**, *216*, 103670. [CrossRef]
30. Burgett, J. An Online Drone Course for Construction Management Students: Curriculum, Simulation, and Certifications. In Proceedings of the 59th Annual Associated Schools, Liverpool, UK, 3–5 April 2023.
31. Cui, J.; Liu, M.; Zhang, Z.; Yang, S.; Ning, J. Robust UAV Thermal Infrared Remote Sensing Images Stitching Via Overlap-Prior-Based Global Similarity Prior Model. *IEEE J. Sel. Top. Appl. Earth Obs. Remote Sens.* **2021**, *14*, 270–282. [CrossRef]
32. Hsieh, C.S.; Hsiao, D.H.; Lin, D.Y. Contour Mission Flight Planning of UAV for Photogrammetric in Hillside Areas. *Appl. Sci.* **2023**, *13*, 7666. [CrossRef]
33. Bento, N.L.; Ferraz, G.A.E.S.; Barata, R.A.P.; Santana, L.S.; Barbosa, B.D.S.; Conti, L.; Becciolini, V.; Rossi, G. Overlap influence in images obtained by an unmanned aerial vehicle on a digital terrain model of altimetric precision. *Eur. J. Remote Sens.* **2022**, *55*, 263–276. [CrossRef]
34. Ahmed, R.; Mahmud, K.H. Potentiality of high-resolution topographic survey using unmanned aerial vehicle in Bangladesh. *Remote Sens. Appl.* **2022**, *26*, 100729. [CrossRef]
35. Ajayi, O.G.; Ogundele, B.S.; Aleji, G.A. Performance evaluation of different selected UAV image processing software on building volume estimation. *Adv. Geod. Geoinf.* **2023**, *72*, e39. [CrossRef]
36. Over, J.S.R.; Ritchie, A.C.; Kranenburg, C.J.; Brown, J.A.; Buscombe, D.D.; Noble, T.; Sherwood, C.R.; Warrick, J.A.; Wernette, P.A. *Processing Coastal Imagery with Agisoft Metashape Professional Edition, Version 1.6-Structure from Motion Workflow Documentation*; US Geological Survey: Reston, VA, USA, 2021.
37. Pham, N.T.; Park, S.; Park, C.S. Fast and Efficient Method for Large-Scale Aerial Image Stitching. *IEEE Access* **2021**, *9*, 127852–127865. [CrossRef]
38. Putri, K.A.; Maulana, M.A. 3D Building Visualization Using LOD1 Level Lidar and Orthophoto Data (Case Study: Jalan Tambak Mayor Surabaya). In Proceedings of the IOP Conference Series: Earth and Environmental Science, Surabaya, Indonesia, 6–11 June 2023; Institute of Physics: Bristol, UK, 2023. [CrossRef]
39. Hazaymeh, K.; Almagbile, A.; Alsayed, A. A cascaded data fusion approach for extracting the rooftops of buildings in heterogeneous urban fabric using high spatial resolution satellite imagery and elevation data. *Egypt. J. Remote Sens. Space Sci.* **2023**, *26*, 245–252. [CrossRef]
40. Tan, Y.; Liang, Y.; Zhu, J. CityGML in the Integration of BIM and the GIS: Challenges and Opportunities. *Buildings* **2023**, *13*, 1758. [CrossRef]
41. El Mghouchi, Y.; El Bouardi, A.; Choulli, Z.; Ajzoul, T. Models for obtaining the daily direct, diffuse and global solar radiations. *Renew. Sustain. Energy Rev.* **2016**, *56*, 87–99. [CrossRef]
42. Oh, M.; Kim, C.K.; Kim, B.; Kang, Y.; Kim, H.G. Real-Time Terrain Correction of Satellite Imagery-Based Solar Irradiance Maps Using Precomputed Data and Memory Optimization. *Remote Sens.* **2023**, *15*, 3965. [CrossRef]
43. Nasser, M.; Hassan, H. Egyptian green hydrogen Atlas based on available wind/solar energies: Power, hydrogen production, cost, and CO_2 mitigation maps. *Int. J. Hydrogen Energy* **2024**, *50*, 487–501. [CrossRef]
44. Greene, C.A.; Gwyther, D.E.; Blankenship, D.D. Antarctic Mapping Tools for MATLAB. *Comput. Geosci.* **2017**, *104*, 151–157. [CrossRef]
45. Nasser, M.; Hassan, H. Feasibility analysis and Atlas for green hydrogen project in MENA region: Production, cost, and environmental maps. *Solar Energy* **2024**, *268*, 112326. [CrossRef]

46. Kaplan, Y.A.; Tolun, G.G.; Batur, E. Developing New Solar Radiation Estimation Models with Machine Learning Techniques and Testing Their Efficiency in Various Places. 2023. Available online: https://www.researchsquare.com/article/rs-3152311/v1 (accessed on 2 April 2024).
47. Mapping Toolbox™ User's Guide R2024a. Version 24.1. 1997. Available online: https://www.mathworks.com/ (accessed on 2 March 2024).
48. Cheng, L.; Zhang, F.; Li, S.; Ju, W.; Li, M. Solar energy potential of urban buildings in 10 cities of China. *Energy* **2020**, *196*, 117038. [CrossRef]
49. Zhu, R.; Wong, M.S.; You, L.; Santi, P.; Ratti, C. The effect of urban morphology on the solar capacity of three-dimensional cities. *Renew. Energy* **2020**, *153*, 1111–1126. [CrossRef]